Nitric Oxide Formation in a Premixed Flame With High-Level Plasma Energy Coupling

Xing Rao, Igor B. Matveev, and Tonghun Lee

Abstract—**This paper presents quantitative planar laser-induced fluorescence (PLIF) imaging of nitric oxide (NO) in a transient-arc direct-current plasmatron igniter using premixed air/fuel mixtures. Quantitative measurements of NO are reported as a function of gas flow rate (20–50 standard cubic feet per hour), plasma power (100–900 mA, 150–750 W), and equivalence ratio (0.7–1.3). Images were corrected for temperature effects by using 2-D temperature field measurements obtained with infrared thermometry and calibrated by a more accurate multiline fitting technique. The signals were then quantified using an NO addition method and spectroscopic laser-induced fluorescence modeling of NO. NO PLIF images and single-point NO concentrations are presented for both plasma-discharge-only and methane/air plasma-enhanced combustion cases. NO formation occurs predominantly through $N_2(v) + O \rightarrow NO + N$ for the plasma-discharge-only case without combustion. The NO concentration for the plasma-enhanced combustion case (500–3500 ppm) was an order of magnitude less than the plasma-discharge-only case (8000–15 000 ppm) due to the reduction of plasma reactions by the methane. Experiments show the linear decay of NO from equivalence ratio 0.8–1.2 under the same flow condition and discharge current.**

Index Terms—**Nitric oxide (NO), plasma torch, plasma-assisted combustion.**

I. INTRODUCTION

DEVELOPMENT and investigation of nonequilibrium plasma discharge for enhancing combustion is receiving increased attention due to its potential application to a variety of problems such as finding a more efficient method of fossil fuel combustion, conversion of low-grade fuels into higher grade fuels, and reduction of pollution through ultralean burn combustion [1], [2]. Advantages of combining plasma discharge with thermal oxidation include faster and more intense chemical energy conversion, increased stability in the lean flammability limit, reduction of pollution by altering oxidation byproducts, improved fuel efficiency through more complete combustion, more reliable and rapid ignition, and stable fuel oxidation across a broader range of pressures and temperatures [3]–[8].

X. Rao and T. Lee are with the Department of Mechanical Engineering, Michigan State University, East Lansing, MI 48823 USA (e-mail: tonghun@msu.edu).

I. B. Matveev is with Applied Plasma Technologies, McLean, VA 22101 USA.

Color versions of one or more of the figures in this paper are available online at http://ieeexplore.ieee.org.

Addition of electromagnetic energy can alter the reaction mechanisms by the following: 1) decomposition of the fuel gas from larger to smaller hydrocarbon molecules and radicals via the electron gas with temperature T_e; 2) radiation-induced electron excitation; 3) increased flame temperature by ohmic heating, which increases the rates of reaction and transport; and 4) increased ion/electrons on key radical initiation and propagation reactions. Recently, Kim *et al.* [9], [10] have shown that fuel reforming into syngas plays a dominant role in stabilization of flames in the presence of a nonequilibrium discharge. A number of different plasma discharges, including thermal plasma discharge [11], dielectric barrier discharge [5], nanosecond pulsed discharge [12], pulsed corona discharge [13], radio frequency discharge [14], dc or low-frequency alternating current discharge [15], and plasmatron [3], gliding arc [16], and microwave discharge [17], have been investigated for enhancing high-temperature thermal oxidation. A more extensive review is available in [1].

Coupling high-temperature reactive flows with a nonequilibrium plasma discharge can lead to significant changes in the formation of nitric oxide (NO), one of the most problematic combustion effluents and a critical design parameter for all practical combustion systems. The key mechanisms involved in the NO chemistry for plasma discharges and methane flames are shown in Table I. Generally, NO formation in conventional combustion is due to four main processes [18], [19]: 1) thermal (Zeldovich) mechanism, which occurs at high temperatures because of the high energy required for dissociation of the nitrogen molecule (reactions 1, 2, and 3); 2) prompt mechanisms with important intermediate species HCN and NH (reactions 4 and 5); 3) N_2O mechanism, which involves third body collision (reactions 6, 7, and 9); and 4) fuel-bound nitrogen mechanism, where nitrogen is supplied from the fuel itself. NO can also be removed by reacting with hydrocarbon radicals in rich flame through a process known as "NO reburn" [20], of which some of the key reactions are also listed in Table I. A slight increase of hydrocarbons in a rich flame can lead to a drastic increase in the reduction of NO. Atomic and molecular excited states reactions also play an important role in formation and reduction of NO [21], [22], and related reactions are shown in Table I.

In the case where no combustion is involved and there is only a plasma discharge, formation of NO from air varies, depending on the discharge system. For example, reaction 14 can be the principal NO formation pathway in pulsed discharge with shorter time scales $(10^{-8}–10^{-6}$ s) [23], while reaction 16 is shown to be dominant in corona discharges [24]. For a variety of reduced electric fields, different percentages

TABLE I
REACTIONS FOR NO FORMATION IN METHANE/AIR FLAME IN PLASMA

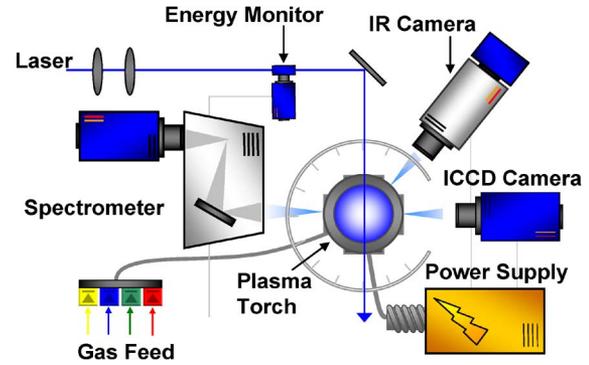|		
Thermal (Zeldovich)mechanism	$O+N_2 \leftrightarrow NO+N$	1
	$N+O_2 \leftrightarrow NO+O$	2
	$OH+N \leftrightarrow NO+H$	3
Prompt mechanisms	$NH+O \leftrightarrow NO+H$	4
	$CN+O_2 \leftrightarrow CO+NO$	5
Mechanism involving N_2O	$O+N_2+M \leftrightarrow N_2O+M$	6
	$N_2O+O \leftrightarrow NO+NO$	7
Other reactions to form NO	$NNH+O \leftrightarrow NO+NH$	8
Electron and Ion Reaction	$N_2+e \leftrightarrow N+N+e$	9
	$N_2O+e \leftrightarrow NO+N+e$	10
	$NO+e \leftrightarrow N+O+e$	11
	$N_2O+e \leftrightarrow N_2+O+e$	12
	$NO_2+e \leftrightarrow NO+O+e$	13
Excited State Species Reaction (*: excited state)	$O+N_2^* \leftrightarrow NO+N$	14
	$NO_2+N_2^* \leftrightarrow NO+N_2+O$	15
	$N(^2D)+O_2 \leftrightarrow NO+O$	16
NO Reburn mechanism	$HCCO + NO \leftrightarrow HCN + CO_2$	17
	$HCCO + NO \leftrightarrow HCNO + CO$	18
	$CH + NO \leftrightarrow HCN + O$	19
	$CH_3 + NO \leftrightarrow HCN + H_2O$	20
	$CH_3 + NO \leftrightarrow H_2CN + OH$	21
	$NH_2+NO \leftrightarrow N_2+H_2O$	22

Fig. 1. Overall experimental setup with synchronization of lasers, energy monitor, ICCD camera, spectrometer, and control system.

the combustion chemistry in the main combustor. Analyzing the NO formation in the main combustor is not a focus of this study, and the goal is to analyze the NO formation only at the tip of the igniter, where the coupling between the reaction zone and the plasma discharge is most pronounced. The conditions in the igniter are unique as the plasma coupling occurs with high levels of power ($\sim$10%–50%), and flow speeds are generally fast and outside the range where a stable flame can be naturally stabilized. Note that the plasma power in the igniter will only be a small fraction of the main combustor. The results presented here are based on our previous conference report [26], with major improvements in the data analysis and interpretation.

of energy deposition into air go to elastic losses, ionization, N_2/O_2 electronic states, and N_2/O_2 vibration [25], resulting in different pathways for NO formation.

In plasma-assisted combustion, analysis of the NO formation mechanism becomes difficult to determine as energy distribution of individual molecules can deviate from thermal equilibrium and the relationship between the NO production and deposition of heat is unclear. More importantly, the high electron density generated by the electric field gives rise to new electron and ion impact processes that can enhance the propagation and branching of radicals and ultimately accelerate NO production. NO formation in plasma-assisted combustion could be formed both from the thermal mechanism due to high combustion temperature and plasma particle reactions, particularly reactions 14, 15, and 16 due to the high energy required for dissociation of nitrogen. As NO formation is a major concern for all practical combustion systems, accurate methods of measuring NO formation in the reaction zone is important to the continued development of plasma-enhanced combustion systems, and a task that can benefit from the extensive research is already available on NO formation of both combustion and plasma systems, respectively.

The main goal of this study is to present and demonstrate quantitative 2-D imaging of NO concentrations in the reaction zone of a transient-arc plasmatron igniter over a wide range of operating conditions using planar laser-induced fluorescence (PLIF) imaging, as well as to predict the main pathway for NO formation. This type of igniter is generally a component of a larger combustion system and plays the role of initiating

II. EXPERIMENTAL SETUP

A general schematic of the laser diagnostics setup is shown in Fig. 1. The excitation of NO using $A_2\Sigma^+ - X_2\Pi(0,0)$ transition requires narrowband UV light near 226 nm. The measurements were conducted using a dye laser (Sirah Precisionscan-LG-2400) with two-stage amplification. Coumarin 450 from Exciton was used for generating pulses at 452 nm, which is frequency doubled through a β-BaB_2O_4 crystal to a final output frequency of 226.03 nm. Laser pulse energy ranged from 7 to 10 mJ/pulse with a 7-ns pulse duration. The laser is pulsed at 10 Hz with a final line width of 0.2 cm^{-1} at 226.03 nm. For spectrally resolved 1-D imaging of the laser-induced fluorescence (LIF) emission, the beam is weakly focused (diameter $\sim$1.5 mm) along a line 20 mm above the top of the torch. The pulse energy is recorded digitally using a fast photodiode (LaVision).

The fluorescence signals were collected at a right angle to the incident laser beam and focused using an $f = 105$ mm f/4.5 achromatic UV lens (UV Nikorr 105), dispersed spectrally through an imaging spectrometer (Acton SP-2300) and imaged onto an intensified camera system composed of a intensified relay optic (LaVision IRO) and charge-coupled device (CCD) camera (LaVision Imager Intense Pro). The resulting image shows the laser path propagating through the flame on the vertical axis and the spectral resolution on the $\times$ axis as shown in Fig. 2 (upper portion). It should be noted that the emission wavelength region coincides with the emission from the Schumann Runge bands of O_2. To quantify this effect, the emission spectra of NO LIF in Fig. 2 have been separated into various components using a nonlinear fitting scheme (using numerical
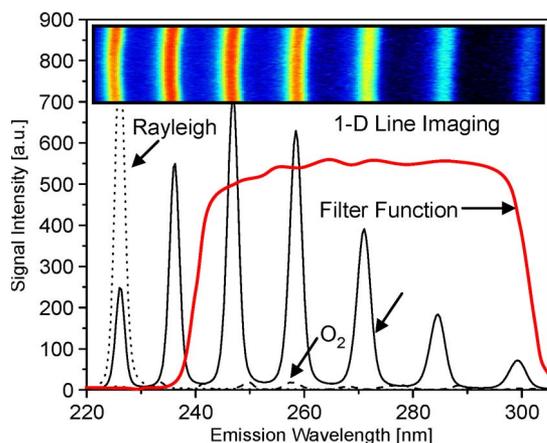
Fig. 2.   Spectrally resolved 1-D line imaging (inset) and the emission spectra of NO-LIF with 226.03 nm excitation and selected filter function (solid red line). The emission spectra has contributions from NO, O_2, and Rayleigh scattering.
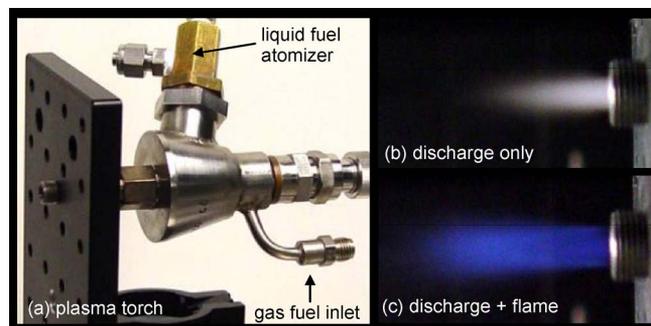

Fig. 3.   (a) Imaging and schematic of transient-arc plasmatron with gas/liquid feeding. (b) Air plasma imaging at 20 SCFH and 300 mA. (c) Plasma-assisted stoichiometric methane/air imaging at 20 SCFH and 300 mA.

emission model [27]) and show the potential contribution from O_2. Therefore, selection of an excitation line with minimized O_2 contribution should be considered.

For PLIF imaging, the laser was optically stretched into a vertical sheet (0.5×35 mm) and imaged directed using the intensified camera with a set of filters for suppression of Rayleigh scattering.

A high-pass interference filter at 240 nm (Asahi Optics) was used for suppression of the Rayleigh scattering, and a low-pass filter at 300 nm (Asahi Optics) was superimposed to cut off any red shift emission past 290 nm was shown in Fig. 2. It should be noted that the spectral shape of NO LIF emission spectra strongly depends on rotational state that NO is excited to [28], with the upper excited state generally not reaching thermal equilibrium within the fluorescence lifetime. Therefore, to avoid effects of nonequilibrium excited-state population effects, broadband detection or one or more complete vibrational bands is preferred.

The full resolution of our camera was 1024×1376, which was binned $2\times$ on the vertical axis and $2\times$ on the horizontal axis to provide a resolution of 64 μm by 64 μm resolution per pixel. All the images were shot with a 50-ns gate as to exclude any stray emission and room light. To ensure the spectral accuracy of the laser, scans of neighboring NO lines were conducted before and after each data set and compared to a numerical simulations from LIFSim [27] (described in more detail in Section III-B). No perceivable drift of the wavelength was detected. Additionally, an IR camera (Flir Phoenix PTS) is used for imaging temperature fields.

The plasma igniter in this work, as shown in Fig. 3, is a transient dc discharge system based on the high-voltage-arc plasmatron [15]. The plasmatron has dimensions of 5 mm inner and 10 mm outer diameters with an arc chamber distance of about 2 in. The transient-arc dc system operates on a repetitive glow-to-spark transition mode, offering the advantages of a thermal plasmatron with low average power output and temperature ($T_g < 1200$ K in air plasma, $n_e \sim 10^{14-15}$ cm^{-3}). During glow-to-spark transition ($\sim$100 ns), a short duration spark or diffused channel arises. The torch works mainly in

the glow mode with voltage applied to the cathode (inner electrode) and the surrounding anode. One advantage is that the electrode erosion is less than traditional dc torches due to the lower electrode temperature. Therefore, intensive cooling is not required. Classical dc arc plasmatrons operate using very high current, while this new plasma igniter/plasmatron uses a semiglow discharge with random completed or noncompleted transitions to spark, which results in highly efficient ignition and flame control with relatively low current and, thus, low average power. This spark exists for only about 100 ns, also hence termed as being "transient".

This plasmatron has shown to increase the flammability over a wide range of operating conditions. For example, flame speed with unburned gas temperature of 300 K in a traditional premixed methane/air flame is $S_L = 0.40$ m/s, which can be increased by more than threefold with a current of 300 mA. Fuel/air mixture could be ignited, and combustion can be stabilized at very lean conditions with oxidation occurring with an equivalence ratio as low as 0.1, and even lower. The ignition mechanism is related to the glow-to-spark transition mentioned above. At the low current glow mode, dissipated energy is not high enough to initiate the fast oxidation process of the fuel, but enough to build up a pool of chemically excited species. When glow-to-spark transition occurs, short duration spark or a diffused channel arises, initiating the ignition process. Even with the small energy released by the transition spark or diffused channel, localized energy deposition coupled with chemically active particles lead to rapid initiation of thermal oxidation. Both liquid and gas fuel can be fed directly into the arc chamber, allowing for high-efficiency thermal oxidation without prior hydrocarbon decomposition. In practice, this igniter will be attached to the main combustor to both initiate ignition and sustain combustion for propulsion, fuel reformation, and power generation purposes.

III. RESULTS AND DISCUSSIONS

A. Quantification of NO

Imaging of NO using LIF is a well-established tool in combustion diagnostics [29]. Therefore, we shall omit a detailed discussion of the relevant spectroscopy except to note that we are using an excitation at 226.03 nm, which has been previously noted as being well isolated from interference of
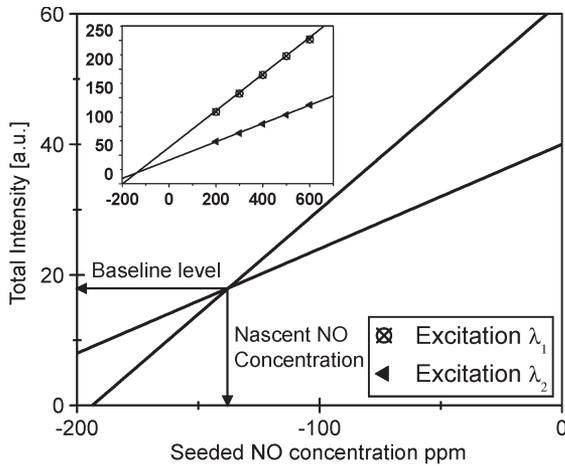
Fig. 4. NO addition method for determination of the baseline strength and the nascent NO concentration.

Fig. 5. Multiline NO LIF thermometry (126 transitions between 225.975 and 226.1 nm).

O_2 [30], [31], even in high-pressure flames where the problem is most pronounced. This excitation line, which is composed of P_1 (23.5), $Q_1 + P_{21}$ (14.5), and $Q_2 + R_{12}$ (20.5) transitions, has a moderate temperature dependence over typical combustion temperatures between 1700 and 2300 K. In this section, we focus on the following three other issues of practical importance: 1) quantification of NO concentration; 2) signal distortion due to thermal nonequilibrium; and 3) signal distortion due to temperature field imaging.

Quantification of the LIF signal can be a difficult task as it is dependent not only on NO number density, but also on the optical setup and potential interference from alternative species. The approach taken here is to calibrate the signal using a well-defined flat flame torch using a variable NO seeding method [32]. The calibration torch is made by fitting a 50-μm sintered plate into a 1-cm-diameter stainless-steel pipe to stabilize a flat 1-D flame and seed various levels of NO. The LIF is measured at two different excitation wavelengths, which have minimal and maximum NO signal strengths, respectively, as illustrated in Fig. 4. The plot shows a magnified view of the small box in the inserted graph. The NO addition is varied from 200 to 600 ppm, and NO LIF is detected with excitation at two different wavelengths. Excitations 1 and 2 refer to two different excitation wavelengths (λ_1: 226.030 nm and λ_2: 226.042 nm).

These wavelengths are selected relatively close together in the target scan range where the baseline intensity, if present, can be assumed to be constant for a given pressure. After measuring the total signal at two different wavelengths at several different NO seeding concentrations, the overall signal is linearly fit as a function of NO seeding for each of the excitation wavelengths. These two linear fits are extrapolated to their intersection yielding the nascent NO concentration and the value of the baseline signal. Determination of the nascent NO concentration (and LIF baseline) by this method assumes that the NO reburn mechanism is first order in NO concentration, as evidenced by the linearity in Fig. 4. In the stoichiometric and lean flames studied here with less than 100 ppm NO addition, the NO reburn is expected to be linear in NO concentration and of no significant amount [33], [34]. It has also been shown that temperature in typical flames does not vary ($\leq 2\%$) for NO
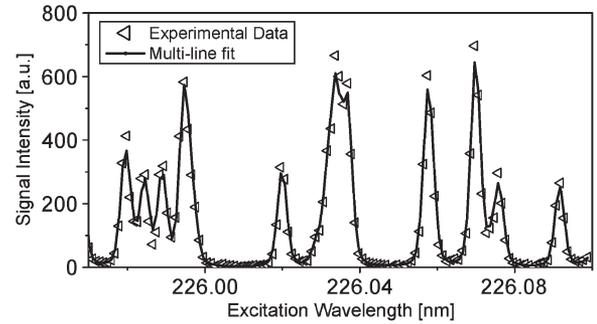
additions as large as 1000 ppm [32]. In all the cases, NO is being weakly excited, and no saturation effects are observed with our laser power.

B. Temperature Profile

One other effect that can significantly influence the LIF signal is the nonequilibrium distribution of the rotational states in the NO. Generally, for most plasma-enhanced combustion systems at atmospheric pressure, it is assumed that the NO in the flame region will follow a Boltzmann distribution of the rotational states and, therefore, in thermal equilibrium. In our studies, this was tentatively confirmed by comparing signal strengths from a number of varying rotational states, where the intensity generally followed the NO concentration within 2%. However, for systems where highly nonequilibrium plasma energy is coupled at lower pressures, the impact of deviation from a thermal equilibrium of the rotational energy E_{rot} on the LIF signal should be considered.

For accurately calibrating the signal intensity for both concentration and spatial variation, we need to acquire information regarding the temperature. It is needed to correct for the temperature variation of the NO LIF signal via the temperature dependence of the laser-excited ground state population, the spectral overlap between the laser-spectral profile and NO absorption spectrum, and the fluorescence yield. In this study, we use IR thermometry for determination of temperature fields, which measure temperature using gray body radiation (infrared) emitted from reacting gases over the whole viewing area. The images are then calibrated at a single point using a multiline NO LIF thermometry [35], which is based on excitation of multiple transitions by scanning the wavelength of the laser over a wide spectral region and then fitting the excitation profile with a numerical simulation. An example of the multiline NO LIF thermometry method is shown in Fig. 5. This provides highly accurate temperatures at a single point which can be used to correct for the less accurate temperature images obtained through the IR thermometry.

The model used for the fitting is LIFSim [27]. LIFSim is a multilevel spectroscopic simulation of NO for the A–X transition during laser absorption and spontaneous fluorescence. It is particularly well calibrated for the $A_2\Sigma^+ - X_2\Pi(0,0)$ transition where the dates for term energies, transition energies, transition strengths, collisional line broadening and shifting, quenching,
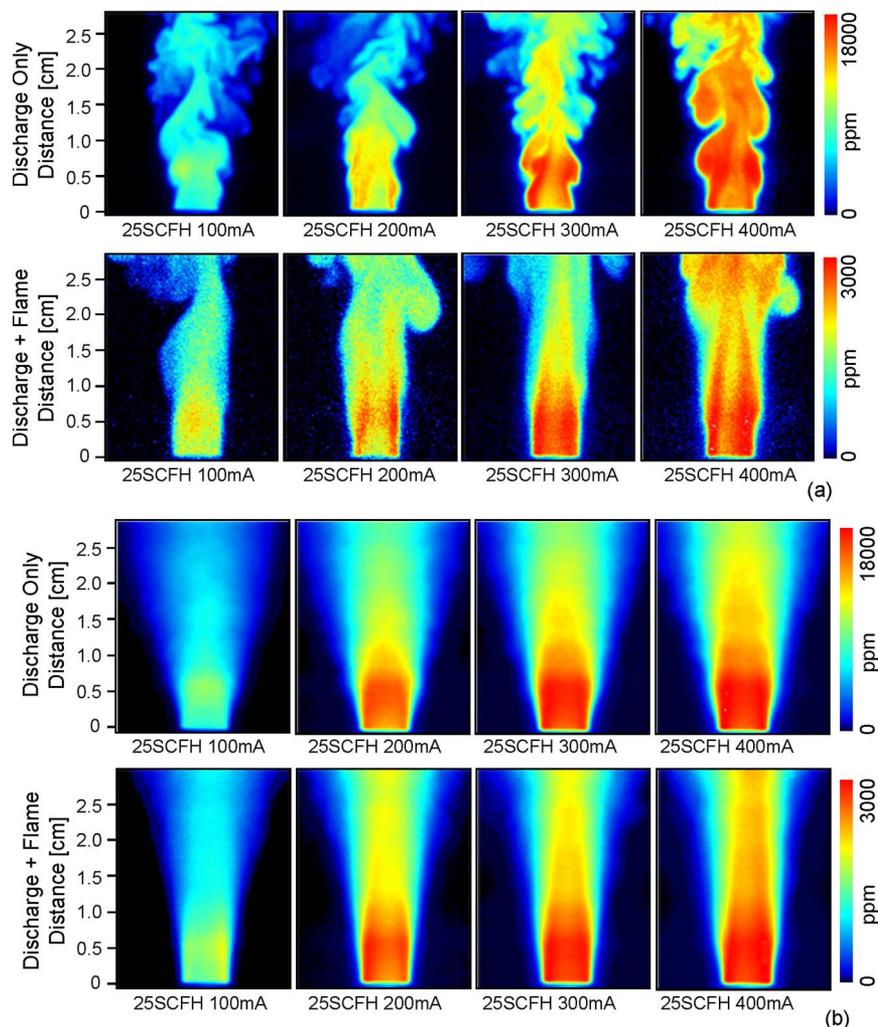
Fig. 6. (a) Single-shot NO concentration fields using NO PLIF of gas discharge of air- and plasma-enhanced flames with different plasma power at the same gas flow rate. (b) Averaged NO concentration fields from NO PLIF (200 images averaged) of plasma-enhanced flames with different plasma power at the same gas flow rate.

and energy transfer terms are well known. For the use of LIFSim in our studies, we must assume thermal equilibrium (or understand subsequent internal energy modes) of the flame, which can be made as the reaction zone outside the torch is far from the arc chamber where all the nonequilibrium effects are dominant. LIFSim is also used to account for temperature dependence of the LIF signal as will be discussed in the following sections.

C. PLIF Imaging of NO

Two-dimensional NO PLIF images are taken for discharge only in air without combustion over a range of flow rates and discharge powers. For plasma-enhanced methane/air combustion, images are taken as a function of flow rate, discharge power, and equivalence ratio. The laser sheet propagates through the center of the plasma torch exit, and the emission is synchronized with the intensified CCD (ICCD) camera. To correct for the laser energy fluctuations, every image is calibrated by the corresponding laser pulse energy, collected using a fast speed photodiode (LaVision). As the gas flow is turbulent,

200 images were averaged when comparing the NO formation for different operating conditions. Averaged images also allow us to accurately calibrate the signal over the imaging field as a function of temperature by using averaged IR thermometry.

Two-dimensional NO PLIF signal intensity is affected not only by the laser pulse power, but also by the nonuniformities in the laser sheet profile and from the spherical aberration of the lens. Emission from a fluorescent UV glass was used for the laser sheet corrections, and the spherical aberration is corrected using an algorithm from the Davis software (LaVision) based on a preshot grid. Both single-shot and averaged 2-D NO concentration images from NO PLIF of discharge only in air as a function of different plasma power and stoichiometric methane/air flame with different plasma power are shown in Fig. 6. In both figures, you can observe the two plasma plumes coming out from either side of the torch.

It can be seen in Fig. 6 that turbulent flows exists in both discharge-only and plasma-enhanced combustion cases for our plasmatron. The degree of instability is observed to be more severe in plasma-discharge-only cases for the same conditions, as the plasma-assisted combustion is more energetically driven
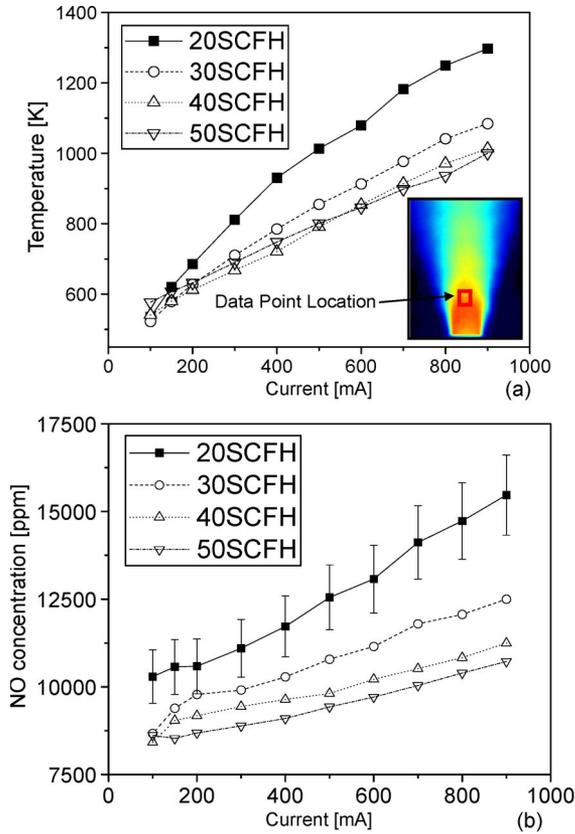
Fig. 7. (a) Temperature and (b) NO concentration data at a specific location of discharge for different power levels and air flow rates in the discharge-only case in air.

by the additional chemical heat release. For the single-shot images, it can be seen that the plasma-only case (upper) row has images that are smoother in quality due to the higher levels of the NO signal, which results in a higher signal-to-noise ratio. Additionally, it should be noted that the NO formed near the flame front is diffused along with the flow and is reduced by about 30%–40% from the highest concentration to a distance of 2.5 cm from the plasmatron exit.

D. Temperatures and NO Concentrations in Plasma Discharge Without Combustion

To compare the NO formation between different operating conditions, we present both temperature and NO concentration at a specific location in our image as shown in Fig. 7 for a plasma-discharge-only case. The location was chosen as a single point in the center of the flame where a stable and high-temperature region exists due to the convergence of the two plasma plumes from either side of the torch. To obtain the temperature at this location, multiline NO LIF thermometry is used for higher accuracy.

NO concentration in the discharge plasma is quantified by the following process. First, the NO LIF intensity value (calibrated for both laser sheet nonuniformity and laser pulse energy) is taken from an averaged image of 200 laser shorts. Using the temperature information provided from NO LIF thermometry, the signal is calibrated for temperature dependence of the NO

excitation by using a multilevel excitation and fluorescence model, LIFSim [27]. Note that we have verified that we are in the linear (weak) excitation region and free from saturation effects. The LIF signal at this point is linear to the number density of NO (in molecules per cubic centimeter), and we apply the following relationship to convert it into a mole fraction based concentration (molecules/total molecules). The final signal is then quantified using an NO addition method previously described in Section III-A. We have

$$I_{\text{LIF}} \sim N_{\text{NO}} = X_{\text{NO}} \times \frac{p}{kT}. \tag{1}$$

I_{LIF} is NO LIF signal intensity, N_{NO} is the number density, and X_{NO} is the mole fraction of NO.

The uncertainty in the temperature measurements affects the concentration measurements through the mole fraction/number density correction in equation (1), and also through calibration of the LIF signal temperature dependence using LIFSim. The temperature uncertainty is within 1% for our measurement techniques at atmospheric pressure. This is because the quenching terms in LIFSim for the low temperatures as that in the plasma discharge has larger errors. The uncertainty associated with beam energy fluctuation corrections and wavelength shift of the laser is expected to be is less than 1%. Camera readout error was suppressed by subtracting a background image taken without the laser pulse and can be neglected. Another component of uncertainty comes from the fact that the quenching coefficient used to determine the LIF strength in LIFSim lacks accuracy at low temperatures in the discharge-only case ($< 5\%$). Combined with the errors from the flowmeters and shot noise (due to statistical fluctuation of a finite number of signal photos reaching the CCD array), the overall uncertainty is expected to be $\sim 7.4\%$ in the NO concentration measurements for plasma discharge and $\sim 4.7\%$ for plasma-assisted combustion.

Fig. 7 shows temperature and NO concentration plots with different gas flow [20–50 standard cubic feet per hour (SCFH)] and average current (100–900 mA). The temperature and NO concentration data are extracted from a region 10 mm from the top of the plasma torch with an area of 2.56 mm $\times$ 2.56 mm (40 pixel $\times$ 40 pixel with resolution of 64 μm$\times$ 64 μm per pixel). The amount of NO production is significantly large due to the large energy input (200–700 W). As the temperature range for all conditions lies within 550–1300 K, NO production from the thermal mechanism is considered to be small in this low temperature range. Moreover, the system lacks carbon and hydrogen compounds required for prompt NO production. Therefore, we can conclude that the possible dominant NO production mechanism is the electron and excited state species (i.e., oxygen) impact reactions, which lead to dissociation of N_2 as well as to possible NO formation reactions from N_2O. In Fig. 7(b), NO production increases with current/power and inversely with air flow. The same general trend is shown in the temperature plot. As formation of NO from N_2O is expected to increase as temperature is decreased, it seems to be of little impact here, indicating that the most dominant mechanism for NO production is the electron, ion, and excited state species impact reactions.

TABLE II
ENERGY DATA OF DISCHARGE ONLY IN AIR WITH DIFFERENT CURRENTS

Current	mA	100	150	200	300	400	500	600	700	800	900
Final Temperature	K	540	630	710	830	920	990	1050	1080	1170	1210
Voltage	kV	1.95	1.55	1.32	0.99	0.8	0.68	0.60	0.54	0.49	0.44
Discharge Power	J/s	195	232.5	264	297	320	340	360	378	392	396
Power for heating	J/s	48	65	83	112	132	148	163	171	193	203
Percentage for heating	%	24.5	28.0	31.3	37.6	41.3	43.5	45.3	45.2	49.2	51.2

It is apparent in Fig. 7(a) that temperature increases with current as a result of more energy per volume of gas. At the same time, temperature drops when the air flow is raised as the gas resident time in the discharge is reduced, leading to fewer collisions between excited particles and eventual lowering of the temperature even though the discharge power is actually higher at higher flow rates due to an increase in the average voltage. The voltage is shown to increase with increased flow rate (not plotted here) in our experimental setup where the flow rate is increased from 20 to 50 SCFH, corresponding to a gas speed increase from 8 to 20 m/s. For all the gas velocities used here, the plasma plume is injected outside the torch and is visually accessible although the initial breakdown is expected to occur inside the torch near the cathode.

For a typical dc discharge, a range between 10^{-5} and 1 A is the normal glow regime, where the voltage will increase as the current increases [36]. Although it is not shown here, we have noticed that the voltage drops in our plasmatron when current is increased for the same flow rate, which leads us to assume weaker electric field but more spark channels to maintain the current. Discharge energy input to the system is not only from the electric field, but also thermal deposition from the higher temperatures. Table II shows the percentage of energy that goes to heating the gas flow at 20 SCFH in a current of 100–900 mA. Energy for heating the plasma gas is calculated using the specific heat C_p of air and assumes that the temperature of the input gas is room temperature of 300 K. It can be seen that the percentage for heating the plasma gas increases with increased current, which also means an increase in the total power input. The increase in the kinetic energy of the molecules and increased collisions further support that NO formation is predominantly from electron and ion impact reactions.

Voltage drop across the plasma column (from the end of the inner cathode) is about 500–1000 V for all the combustion conditions in this study, and the length of the plasma column is about 4 mm. Therefore, the reduced electric field (E/n) is calculated to be 50–85 Td (1 Td = 10^{-17} V·cm²) for 500–1000 V, 1 atm, and 4 mm. Reduced electric field is a measure of kinetic energy transfer cross section from electrons to internal degrees-of-freedom molecules. For certain reduced electric fields, appropriate molecular energy states is excited. For example, vibrational levels of the ground electronic state nitrogen, or low-energy electronic states of oxygen, are more likely to be excited at a lower E/n level, while high-energy electronic levels of nitrogen and oxygen, as well as their dis-

sociation and ionization, are excited at a higher E/n level. For this experiment, majority of the energy deposition into the air results in N_2 molecule vibration (90%–95%) excitation along with some N_2 electronic states (∼5%) while there exists little ionization, rotation, or O_2 vibrational/electric excited states [25]. Therefore, the main pathway responsible for large amount of NO production is $N_2(v) + O \rightarrow NO + N$ in this case. This is consistent with the kinetic model study of a similar dc glow discharge with the same order of magnitude of reduced electric field in [37].

We find that NO production in a dc plasmatron can be significantly high near the reaction zone and that the glow-to-spark transition strongly affects the NO production via an increase in the electron density. This NO formation channel will be interrupted by the methane when combustion is involved, as will be shown in Section III-E.

E. Temperatures and NO Concentrations in a Plasma-Enhanced Flame

We now present results in a plasma-enhanced flame in a similar format as in Section III-D. The NO concentration is shown as a function of current, equivalence ratio, and total flow rate.

Glow-to-spark transition with even little energy dissipation can significantly contribute to the ignition of fuel during plasma-assisted combustion due to the abundance of chemically active particles already present in the glow discharge. This random and continuous transition is then able to sustain the flame. Ignition in the methane/air mixture can be achieved with equivalence ratios as low as 0.1. As stated in the description of plasmatron (Section II), the flame speed of premixed flames in this type of discharge can increase threefold or more at 300 mA, with further increases at higher currents. Also note that in the plasma, energy added is on the order of 15%–95% of the thermal energy from the combustion, which is generally reasonable in an ignition system of this kind. Keep in mind that the power level will be orders of magnitude lower than the actual combustion system that the igniter will be a part of in a practical system.

In Fig. 8, we show the temperature and NO concentration as a function of current and flow rate when the equivalence ratio is held at 1. It is apparent in Fig. 8(a) that the gas temperature increases with current, an indication that the deposition of heat increased when more energy is added to the flow. Unlike the discharge-only case, the temperature goes up with the flow rate. This is due to the heat release of the combustion process,
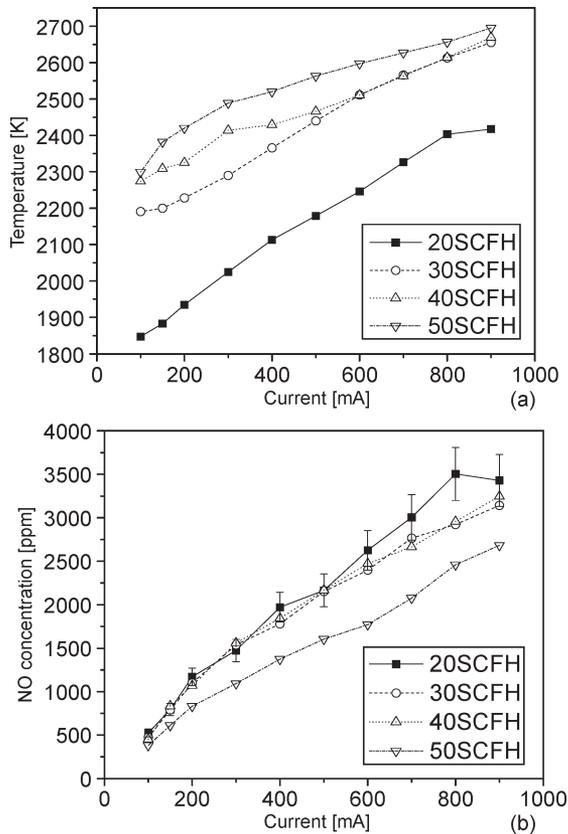
Fig. 8. (a) Temperature and (b) NO concentration data as a function of current and flow rate when the equivalence ratio is held at 1 in plasma-assisted methane/air combustion.
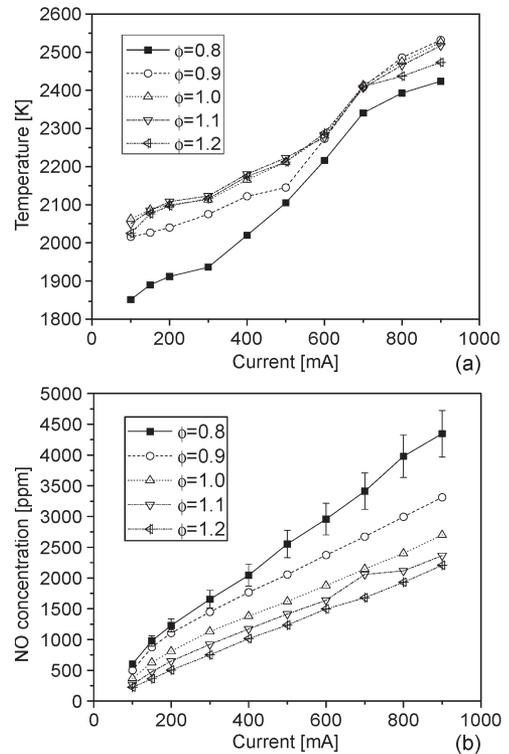

Fig. 9. (a) Temperature and (b) NO concentration data as a function of current and equivalence ratio when the flow rate is held at 25 SCFH in plasma-assisted methane/air combustion.

which increases the temperature of the gas, and although the stoichiometry is maintained, the increased density of the burnt fuel in the confined arc chamber and through the exit of the torch results in a higher temperature. The plasma input power (current × voltage) to the flame is similar in magnitude to that of the plasma-discharge-only case. It can be seen that the NO production is reduced to a much lower level of 500–3500 ppm rather than the 8000–15 000 ppm shown in the discharge-only case. This reduction of NO has also been previously observed by Kim *et al.* [10], [38].

The main cause of this effect is the addition of methane, which is a discharge interruption species (particularly compared to other compositions O_2 and N_2), and alternative electron impact reactions, which lead to reduced NO formation. Note that temperature is high in the plasma-assisted methane/air combustion (1850–2600 K), where thermal NO formation is most likely the dominant mechanism. In particular, we notice in Fig. 8 that NO concentration surprisingly decreases with the flow rate, although this leads to an increase in temperature and injection density of plasma energy into the flow. Upon further inspection, we note that the plasma energy input per molecule is actually decreased as the flow rate is increased from 20 to 50 SCFH. Energy input for each molecule is 0.203, 0.162, 0.159, and 0.154 eV/molecule for 20, 30, 40, and 50 SCFH, respectively, at 100 mA and stoichiometric conditions. This lower power input per molecule at higher flow rate results in less electrons and collisions needed to initiate reactions that

can results in the increase of NO. This is a clear example that although thermal NO is expected to be dominant in the high temperature range here, it is not the only mechanism.

In Fig. 9, the temperature and NO concentration as a function of current and equivalence ratio when flow rate is held at 25 SCFH are shown. It can be seen that the NO increases with the current/power as well as with the total flow rate. Once again, it is interesting to note that NO formation is higher for leaner flames although the temperature is lower. Therefore, in addition to what can be expected from thermal formation of NO, we need to consider the impact of increased methane. This is addressed in the following.

In Fig. 10, we show the temperature and NO concentration as function of equivalence ratio and the flow rate when the current is held at 300 mA. The temperature profile as a function of equivalence ratio is similar to that of a typical case of combustion using methane without any plasma enhancements. The peak temperature is reached at an equivalence ratio close to 1, and higher current/power of the plasma increases the absolute temperature. The temperature for a lower flow rate of methane/air mixture is lower than that of the higher flow rate due to the less chemical heat release from combustion. It is interesting to observe the linear decay of NO as the equivalence ratio is increased. Note that NO quenching cross section with methane is extremely low [39], and therefore, the direction between the two species is negligible. On the other hand, methane will act as a discharge interruption species (particularly compared to other composition O_2 and N_2), and the indirect interaction between methane and discharge will
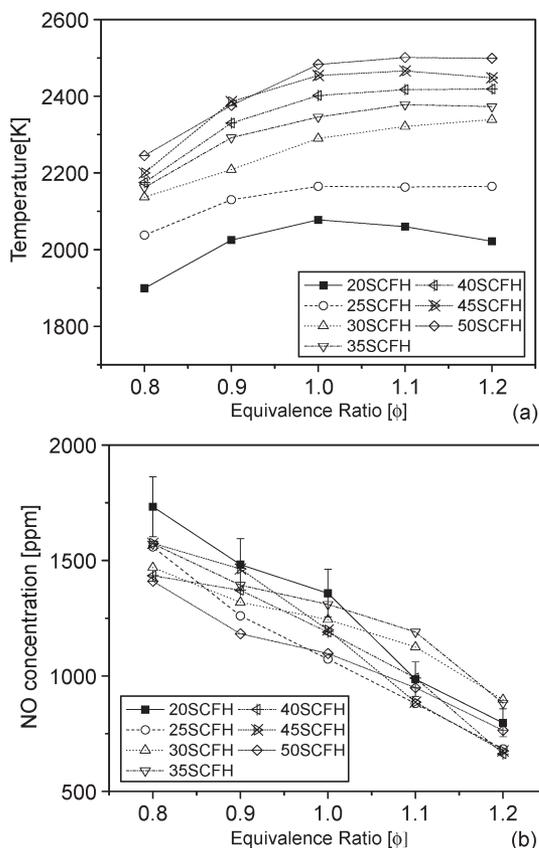
Fig. 10. (a) Temperature and (b) NO concentration data as a function of equivalence ratio and flow rate when the current is held at 300 mA in plasma-assisted methane/air combustion.

significantly impact the NO formation. First, generation of vibrational nitrogen, which is a key factor for NO formation, is reduced even though the same amount of energy is added to the system as greater portion of it is allocated to alternative electron impact reactions, including breaking of CH_4 into smaller molecules. Second, as the flame becomes richer, unburnt hydrocarbons can also contribute to the reduction of NO through reburn reactions. Third, atomic oxygen and ozone generated from hydrocarbon help bring NO level down through reverse Zeldovich reaction $NO + O \rightarrow N + O_2$ and through NO interactions with ozone. Atomic oxygen and ozone can be abundant in hydrocarbon/air mixtures when a plasma discharge is present and have been reported to increase flame propagation speed [2] and enhance flame speed [40]. NO decay mechanism through atomic oxygen and ozone is confirmed experimentally and by using kinetic models in [41]. The main production channel of atomic oxygen is believed to be the dissociative quenching of O_2 [42], [43] by N_2. Another potential explanation can be from the fact that as fuel reforming is increased in the so-called "cold preflame" regions, it competes with NO formation reactions in the use of atomic oxygen, thus leading to the reduction of NO [9], [38]. In actual practice, where this torch will be a part of a larger combustor, the additional chemistry and the fluid dynamics of the combustor will determine the overall NO formation, and the conditions of the igniter should be determined according to the conditions of the specific application.

IV. CONCLUSION

PLIF is used to acquire spatially resolved oxide (NO) concentrations in plasma-enhanced flames of a transient-arc plasmatron. Quantitative concentration of NO is calibrated by comparing the LIF signal to a well-defined flat-flame calibration torch and using an NO addition method.

IR thermometry and a more accurate multiline fitting technique of multiple NO transitions are used to obtain temperature field for the following two purposes: 1) correction of LIF signal due to spectroscopic temperature dependence and 2) investigation of the changes in NO production as a variation of temperature.

Planar LIF images of NO were generated to show relative NO concentration in both cases of plasma only and plasma-enhanced combustion. In the case of plasma only, NO production is high in the region of 8000–15 000 ppm with dc power input of 200–750 W. Temperature range at these conditions is 550–1250 K, where thermal NO production is minor and NO formation is predominantly from $N_2(v) + O \rightarrow NO + N$.

For plasma-enhanced combustion, NO production in methane/air flame for investigated equivalence ratio range is about one order lower in magnitude. In this case, temperature is so high that thermal NO mechanism is still dominant. Plasma power and equivalence ratio are the two main operational parameters in producing NO in the combustion system here. For a lower NO concentration in plasma-enhanced flames of this type, we need to avoid lean and high current conditions. Linear decay from an equivalence ratio of 0.8–1.2 may be caused by the quenching of vibrational nitrogen, interactions with atomic oxygen and ozone, and reaction with unburned hydrocarbon species at rich conditions.

Future study will involve analysis of chemical kinetics modeling and identification of key formation reactions that are impacted by the plasma. This will require measurements being made in a well-defined 1-D flat flame where the concentration can be compared with numerical chemical kinetics simulations using plasma reaction integrated reaction mechanisms.

REFERENCES

[1] S. M. Starikovskaia, "Plasma assisted ignition and combustion," *J. Phys. D, Appl. Phys.*, vol. 39, no. 16, pp. R265–R299, Aug. 2006.
[2] A. Y. Starikovskii, "Plasma supported combustion," *Proc. Combust. Inst.*, vol. 30, no. 2, pp. 2405–2417, Jan. 2005.
[3] L. Bromberg, D. R. Cohn, A. Rabinovitch, and J. Heywood, "Emissions reductions using hydrogen from plasmatron fuel converters," *Int. J. Hydrogen Energy*, vol. 26, no. 10, pp. 1115–1121, Oct. 2001.
[4] S. B. Leonov and D. A. Yarantsev, "Plasma-induced ignition and plasma-assisted combustion in high-speed flow," *Plasma Sources Sci. Technol.*, vol. 16, no. 1, pp. 132–138, Feb. 2007.
[5] W. Kim, H. Do, M. G. Mungal, and M. A. Cappelli, "Plasma-discharge stabilization of jet diffusion flames," *IEEE Trans. Plasma Sci.*, vol. 34, no. 6, pp. 2545–2551, Dec. 2006.

[6] D. H. Lee, K. T. Kim, M. S. Cha, and Y. H. Song, "Optimization scheme of a rotating gliding arc reactor for partial oxidation of methane," *Proc. Combust. Inst.*, vol. 31, no. 2, pp. 3343–3351, Jan. 2006.

[7] T. Ombrello, X. Qin, Y. Ju, A. Gutsol, A. Fridman, and C. Carter, "Combustion enhancement via stabilized piecewise nonequilibrium gliding arc plasma discharge," *AIAA J.*, vol. 44, no. 1, pp. 142–150, Jan. 2006.

[8] A. B. Leonov, D. A. Yarantsev, A. P. Napartovich, and I. V. Kochetov, "Plasma-assisted ignition and flameholding in high-speed flow," presented at the 44th AIAA Aerospace Sciences Meeting, Reno, NV, 2006, Paper AIAA-2006-563.

[9] W. Kim, H. Do, M. G. Mungal, and M. A. Cappelli, "A study of plasma-stabilized diffusion flames at elevated ambient temperatures," *IEEE Trans. Plasma Sci.*, vol. 36, no. 6, pp. 2898–2904, Dec. 2008.

[10] W. Kim, M. G. Mungal, and M. A. Cappelli, "The role of *in situ* reforming in plasma enhanced ultra lean premixed methane/air flames," 2009. DOI:10.1016/j.combustflame.2009.06.016, submitted for publication.

[11] T. Kitagawa, A. Moriwaki, K. Murakami, K. Takita, and G. Masuya, "Ignition characteristics of methane and hydrogen using a plasma torch in supersonic flow," *J. Propuls. Power*, vol. 19, no. 5, pp. 853–858, 2003.

[12] A. Y. Starikovskii, N. B. Anikin, I. N. Kosarev, E. I. Mintoussov, M. M. Nudnova, A. E. Rakitin, D. V. Roupassov, S. M. Starikovskaia, and V. P. Zhukov, "Nanosecond-pulsed discharge for plasma-assisted combustion and aerodynamics," *J. Propuls. Power*, vol. 24, no. 6, pp. 1182–1197, Nov./Dec. 2008.

[13] G. Lou, A. Bao, M. Nishihara, S. Keshav, Y. G. Utkin, J. W. Rich, W. R. Lempert, and I. V. Adamovich, "Ignition of premixed hydrocarbon–air flows by repetitively pulsed, nanosecond pulse duration plasma," *Proc. Combust. Inst.*, vol. 31, no. 2, pp. 3327–3334, Jan. 2007.

[14] N. Chintala, A. Bao, G. Lou, and I. V. Adamovich, "Measurements of combustion efficiency in nonequilibrium RF plasma-ignited flows," *Combust. Flame*, vol. 144, no. 4, pp. 744–756, Mar. 2006.

[15] Y. D. Korolev and I. B. Matveev, "Nonsteady-state processes in a plasma pilot for ignition and flame control," *IEEE Trans. Plasma Sci.*, vol. 34, no. 6, pp. 2507–2513, Dec. 2006.

[16] I. V. Kuznetsova, N. Y. Kalashnikov, A. F. Gutsol, A. F. Fridman, and L. A. Kennedy, "Effect of 'overshooting' in the transitional regimes of the low-current gliding arc discharge," *J. Appl. Phys.*, vol. 92, no. 8, pp. 4231–4237, Oct. 2002.

[17] S. H. Zaidi, E. Stockman, X. Qin, Z. Zhao, S. Macheret, Y. Ju, R. B. Miles, D. J. Sullivan, and J. F. Kline, "Measurements of hydrocarbon flame speed enhancement in high-Q microwave cavity," presented at the 44th AIAA Aerospace Sciences Meeting and Exhibit, Reno, NV, 2006, Paper AIAA-2006-1217.

[18] C. T. Bowman, "Gas-phase reaction mechanisms for nitrogen oxide formation and removal in combustion," in *Pollutants from Combustion*, C. Vovelle, Ed. Amsterdam, The Netherlands: Kluwer, 2000, pp. 123–144.

[19] J. Warnatz, U. Maas, and R. W. Dibble, *Combustion,* 3rd ed. Berlin, Germany: Springer-Verlag, 1997.

[20] B. Atakan and A. T. Hartlieb, "Laser diagnostics of NO reburning in fuel-rich propene flames," *Appl. Phys. B, Lasers Opt.*, vol. 71, no. 5, pp. 697–702, Nov. 2000.

[21] I. Orlandini and U. Riedel, "Modelling of NO and HC removal by non-thermal plasmas," *Combust. Theory Model.*, vol. 5, no. 3, pp. 447–462, Sep. 2001.

[22] L. Magne, S. Pasquiers, N. Blin-Simiand, and C. Postel, "Production and reactivity of the hydroxyl radical in homogeneous high pressure plasmas of atmospheric gases containing traces of light olefins," *J. Phys. D, Appl. Phys.*, vol. 40, no. 10, pp. 3112–3127, May 2007.

[23] J. T. Herron, "Modeling studies of the formation and destruction of NO in pulsed barrier discharges in nitrogen and air," *Plasma Chem. Plasma Process.*, vol. 21, no. 4, pp. 581–609, Dec. 2001.

[24] G. Zhao, S. V. B. Janardhan, X. Hu, M. D. Argyle, and M. Radosz, "Effect of oxygen on nonthermal plasma reactions of nitrogen oxides in nitrogen," *AIChE J.*, vol. 51, no. 6, pp. 1800–1812, 2005.

[25] A. Bao, "Ignition of hydrocarbon fuels by a repetitively pulsed nanosecond pulse duration plasma," Ph.D. dissertation, Dept. Mech. Eng., Ohio State Univ., Columbus, OH, 2008.

[26] X. Rao, T. Lee, and I. Matveev, "Nitric oxide formation during ignition and combustion of a transient arc plasmatron," presented at the 47th AIAA Aerospace Sciences Meeting, Orlando, FL, 2009, Paper AIAA 2009-280.

[27] W. G. Bessler, C. Schulz, V. Sick, and J. W. Daily, "A versatile modeling tool for nitric oxide LIF spectra," in *Proc. 3rd Joint Meeting U.S. Sec. Combust. Inst.*, Chicago, IL, 2003.

[28] C. Schulz, V. Sick, U. E. Meier, J. Heinze, and W. Stricker, "Quantification of NO A-X (0, 2) laser-induced fluorescence: Investigation of calibration and collisional influences in high-pressure flames," *Appl. Opt.*, vol. 38, no. 9, pp. 1434–1443, 1999.

[29] K. Kohse-Höinghaus and J. B. Jeffries, *Applied Combustion Diagnostics*. New York: Taylor & Francis, 2002.

[30] M. D. DiRosa, K. G. Klavuhn, and R. K. Hanson, "LIF spectroscopy of NO and O_2 in high-pressure flames," *Combust. Sci. Technol.*, vol. 118, no. 4–6, pp. 257–283, Oct. 1996.

[31] W. G. Bessler, C. Schulz, T. Lee, J. B. Jeffries, and R. K. Hanson, "Strategies for laser-induced fluorescence detection of nitric oxide in high-pressure flames. III. Comparison of A-X excitation schemes," *Appl. Opt.*, vol. 42, no. 24, pp. 4922–4936, 2003.

[32] T. Lee, W. G. Bessler, H. Kronemayer, C. Schulz, and J. B. Jeffries, "Quantitative temperature measurements in high-pressure flames with multiline NO-LIF thermometry," *Appl. Opt.*, vol. 44, no. 31, pp. 6718–6728, 2005.

[33] P. A. Berg, G. P. Smith, J. B. Jeffries, and D. R. Crosley, "Nitric oxide formation and reburn in low-pressure methane flames," *Proc. Combust. Inst.*, vol. 27, pp. 1377–1384, 1998.

[34] J. H. Bromly, F. J. Barnes, S. Muris, X. You, and B. S. Haynes, "Kinetic and thermodynamic sensitivity analysis of the NO-sensitised oxidation of methane," *Combust. Sci. Technol.*, vol. 115, no. 4–6, pp. 259–296, Jun. 1996.

[35] W. G. Bessler and C. Schulz, "Quantitative multi-line NO-LIF temperature imaging," *Appl. Phys. B, Lasers Opt.*, vol. 78, no. 5, pp. 519–533, Mar. 2004.

[36] A. Fridman and L. Kennedy, *Plasma Physics and Engineering*. New York: Taylor & Fancis, 2004.

[37] B. F. Gordiets, C. M. Ferreira, V. L. Guerra, J. M. A. H. Loureiro, J. Nahorny, D. Pagnon, M. Touzeau, and M. Vialle, "Kinetic model of a low-pressure N_2-O_2 flowing glow discharge," *IEEE Trans. Plasma Sci.*, vol. 23, no. 4, pp. 750–768, Aug. 1995.

[38] W. Kim, H. Do, M. G. Mungal, and M. A. Cappelli, "Investigation of NO production and flame structure in plasma enhanced premixed combustion," *Proc. Combust. Inst.*, vol. 31, no. 2, pp. 3319–3326, Jan. 2007.

[39] M. C. Drake and J. W. Ratcliffe, "High temperature quenching cross sections for nitric oxide laser-induced fluorescence measurements," *J. Chem. Phys.*, vol. 98, no. 5, pp. 3850–3865, 1993.

[40] T. Ombrello, S. H. Won, Y. Ju, and S. Williams, "Lifted flame speed enhancement by ozone," in *Proc. 4th Int. Workshop Exhib. Plasma Assisted Combust.*, 2008, pp. 17–19.

[41] M. Uddi, N. Jiang, I. V. Adamovich, and W. R. Lempert, "Nitric oxide density measurements in air and air/fuel nanosecond pulse discharges by laser induced fluorescence," *J. Phys. D, Appl. Phys.*, vol. 42, no. 7, p. 075 205, Mar. 2009.

[42] G. D. Stancu, F. Kaddouri, D. A. Lacoste, and C. O. Laux, "Investigations of rapid plasma chemistry generated by nanosecond discharges in air at atmospheric pressure using advanced optical diagnostics," in *47th AIAA Aerospace Sciences Meeting*, Orlando, FL, 2009.

[43] M. Uddi, N. Jiang, E. Mintusov, I. V. Adamovich, and W. R. Lempert, "Atomic oxygen measurements in air and air/fuel nanosecond pulse discharge by two photon laser induced fluorescence," *Proc. Combust. Inst.*, vol. 32, no. 1, pp. 929–936, 2009.
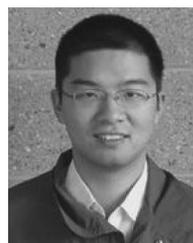
Xing Rao was born in Jinxi, China, on March 26, 1985. He received the B.S. degree in mechanical engineering and the M.S. degree in nuclear engineering from Tsinghua University, Beijing, China, in 2005 and 2007, respectively. He is currently working toward the Ph.D. degree with Michigan State University, East Lansing.

He is currently a Graduate Research Assistant with Michigan State University. His research interests include laser diagnostics in plasma-assisted combustion and energetic nanoparticle-enhanced combustion.

Mr. Rao is a Student Member of the American Institute of Aeronautics and Astronautics and the Combustion Institute.

Igor B. Matveev was born in Samara, Russia, on February 11, 1954. He received the M.S. and Ph.D. degrees in mechanical engineering from the Nikolaev Shipbuilding Institute, Nikolaev, Ukraine, in 1977 and 1984, respectively. His Ph.D. thesis was entitled, "Development and implementation of the plasma ignition systems for naval gas turbines."

From 1977 to 1990, he was a Researcher, a teacher, and an Associate Professor with the Nikolaev Shipbuilding Institute. In 1990, he established Plasmatechnika Ltd., a privately owned company for the development and mass production of plasma systems. Since 2003, he has been with Applied Plasma Technologies, McLean, VA, where he is the President and CEO. His current research interests include novel PAC technologies and their development and implementation.
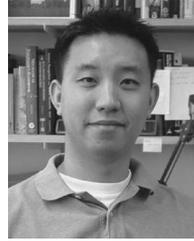
Tonghun Lee was born in Seoul, Korea, on April 3, 1974. He received the B.S. degree in mechanical engineering from Yonsei University, Seoul, Korea, in 2000 and the M.S. and Ph.D. degrees in mechanical engineering from Stanford University, Stanford, CA, in 2002 and 2006, respectively.

He is currently an Assistant Professor with the Department of Mechanical Engineering, Michigan State University, East Lansing. His research interests include laser diagnostics of high-pressure combustion systems, plasma-enhanced flames, as well as oxidation of novel biofuels. His research group at Michigan State University is devoted to fundamental research in applying laser-based optical methods for the development of advanced combustion and propulsion system technologies.